

Arnaud Jollivet, François H. Julien, Borislav Hinkov, Stefano Pirotta, Sophie Derelle, Julien Jaeck, Maria Tchernycheva, Raffaele Colombelli, Adel Bousseksou, Maxime Hugues, Nolwenn Le Biavan, Julen Tamayo-Arriola, Miguel Montes Bajo, Gottfried Strasser, Jean-Michel Chauveau, Adrian Hierro, "Short infrared wavelength quantum cascade detectors based on non-polar ZnO/ZnMgO quantum wells," Proc. SPIE 10919, Oxide-based Materials and Devices X, 1091919 (1 March 2019)

Copyright 2019 Society of Photo-Optical Instrumentation Engineers. One print or electronic copy may be made for personal use only. Systematic reproduction and distribution, duplication of any material in this paper for a fee or for commercial purposes, or modification of the content of the paper are prohibited.

<http://dx.doi.org/10.1117/12.2507768>

# PROCEEDINGS OF SPIE

[SPIDigitalLibrary.org/conference-proceedings-of-spie](https://spiedigitallibrary.org/conference-proceedings-of-spie)

## Short infrared wavelength quantum cascade detectors based on non-polar ZnO/ZnMgO quantum wells

Arnaud Jollivet, François H. Julien, Borislav Hinkov, Stefano Pirotta, Sophie Derelle, et al.

Arnaud Jollivet, François H. Julien, Borislav Hinkov, Stefano Pirotta, Sophie Derelle, Julien Jaeck, Maria Tchernycheva, Raffaele Colombelli, Adel Bousseksou, Maxime Hugues, Nolwenn Le Biavan, Julien Tamayo-Arriola, Miguel Montes Bajo, Gottfried Strasser, Jean-Michel Chauveau, Adrian Hierro, "Short infrared wavelength quantum cascade detectors based on non-polar ZnO/ZnMgO quantum wells", Proc. SPIE 10919, Oxide-based Materials and Devices X, 1091919 (1 March 2019); doi: 10.1117/12.2507768

**SPIE.**

Event: SPIE OPTO, 2019, San Francisco, California, United States

# Short infrared wavelength quantum cascade detectors based on non-polar ZnO/ZnMgO quantum wells

Arnaud Jollivet<sup>1</sup>, François H. Julien<sup>1</sup>, Borislav Hinkov<sup>2</sup>, Stefano Pirotta<sup>1</sup>, Sophie Derelle<sup>3</sup>, Julien Jaeck<sup>3</sup>, Maria Tchernycheva<sup>1</sup>, Raffaele Colombelli<sup>1</sup>, Adel Bousseksou<sup>1</sup>, Maxime Hugues<sup>4</sup>, Nolwenn Le Biavan<sup>4</sup>, Julen Tamayo-Arriola<sup>5</sup>, Miguel Montes Bajo<sup>5</sup>, Gottfried Strasser<sup>2</sup>, Jean-Michel Chauveau<sup>4</sup>, Adrian Hierro<sup>5</sup>

<sup>1</sup> Center of Nanoscience and Nanotechnology, C2N, Univ. Paris-Sud, University Paris-Saclay, Palaiseau, France.

<sup>2</sup> TU-Wien, Nanocenter Campus-Gußhaus, Gußhausstraße 25, Gebäude-CH, A-1040 Vienna, Austria.

<sup>3</sup> ONERA/DOTA/CIO, Chemin de la Hunière, 91761 Palaiseau Cedex, France.

<sup>4</sup> Université Côte d'Azur, CNRS, CRHEA, 06560 Valbonne, France.

<sup>5</sup> Instituto de Sistemas Optoelectrónicos y Microtecnología, Univ. Politécnica de Madrid, Madrid Spain.

## ABSTRACT

We report on the first demonstration of quantum cascade detectors based on ZnO/ZnMgO quantum wells grown by molecular beam epitaxy on an m-plane ZnO substrate. The sample is processed in the form of square mesas with special attention paid to the passivation of the side facets. Photocurrent spectroscopy reveals a resonance at 2.8  $\mu\text{m}$  wavelength slightly blue-shifted with respect to the intersubband absorption peak at 3  $\mu\text{m}$  wavelength. The photocurrent persists up to room temperature. The peak responsivity amounts to 0.15 mA/W under irradiation at Brewster's angle of incidence of the top surface of the mesas.

## 1. INTRODUCTION

Wurzite ZnO/ZnMgO is appearing as a new material for intersubband (ISB) devices. First observation of ISB absorption in this material system has been reported for c-plane quantum well (QW) structures.<sup>1</sup> However, these QWs are the siege of huge internal electric fields because of the polarization discontinuity and between the well and barrier materials. Recently m-plane ZnO/ZnMgO heterostructures have opened new prospects for ISB devices.<sup>2</sup> Indeed, the absence of internal electric field for this particular orientation greatly simplifies the design of quantum cascade devices. This is the case for quantum cascade detectors (QCD).

QCDs are photovoltaic devices.<sup>3,4</sup> With respect to quantum well infrared (QWIPs) photoconductors, the absence of dark current in QCDs is a key point for enhancing the signal-to-noise ratio. As illustrated in Figure 1, one stage of the multi-period active region of a QCD device consists of an active quantum well, where the ISB absorption takes place, and an extractor stage whose purpose is to transfer the photoexcited electrons from the active QW to the next period active QW. As a result, a photovoltage is generated across the device which can translate in a photocurrent if the device is connected to a load resistor. The design of the extractor stage usually relies on multiple QWs to achieve a staircase of bound electronic states separated by the energy of one longitudinal optical (LO) phonon in order to benefit from an efficient electron LO-phonon scattering between the states. So far, QCDs have been demonstrated in the arsenide, antimonide, III-nitride and ZnCdSe/ZnCdMgSe material systems in the wavelength range from 1 to 84  $\mu\text{m}$ .<sup>3,12</sup>

The detectivity of a QCD is proportional to the square root of the resistance at zero bias ( $R_0$ ) times the area of the detector ( $A$ ).<sup>3</sup>  $R_0$  is limited by the non-resonant electron tunneling from the ground state of the active QW to one of the extractor states assisted by the absorption of LO-phonons.<sup>13</sup> In highly polar materials like ZnO, the Frölich interaction between electrons and LO-phonons is strongly enhanced leading to an enhanced electronic transfer efficiency within the extractor. A further appealing feature of QCDs is their fast intrinsic response.<sup>13</sup> GaN-based QCDs operating at 1.5  $\mu\text{m}$  wavelength have revealed a -3 dB frequency bandwidth exceeding 40 GHz.<sup>14</sup> It should be noticed that no QCD based on ZnO heterostructures has been reported so far.

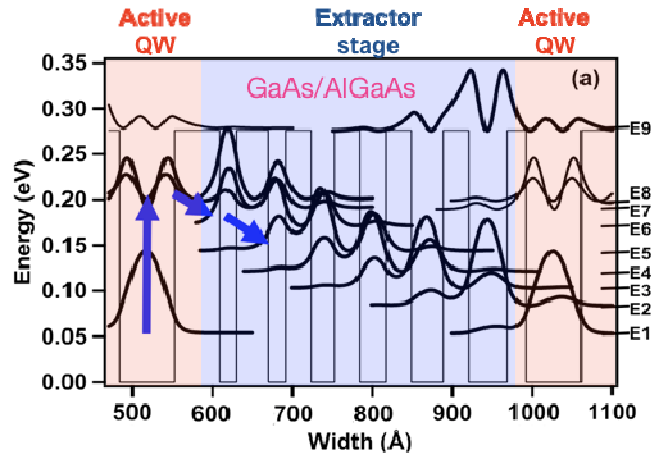


Figure 1. Conduction band profile of a GaAs/AlGaAs QCD from Ref [3].

This paper reports on the first demonstration of the QCDs based on ZnO/ZnMgO m-plane heterostructures. The samples were grown by molecular beam epitaxy (MBE) on m-plane ZnO substrates. ISB absorption spectroscopy using a Fourier Transform Infrared (FTIR) spectrometer reveals the TM-polarized ISB absorption is peaked at 3  $\mu\text{m}$  wavelength. QCD devices has been processed in the form of 260 square mesas with a size ranging from  $10 \times 10 \mu\text{m}^2$  up to  $100 \times 100 \mu\text{m}^2$ . Special attention has been dedicated to the mesa facet passivation. I-V characteristics reveal that 86% of the devices are operational. The current density versus voltage is independent of the mesa size at room temperature which is indicative of the absence of surface leakage currents. In contrast, at a temperature of 77 K, electron leakage through the mesa sidewalls dominates the transport. Photocurrent spectroscopy of  $100 \times 100 \mu\text{m}^2$  QCDs has been performed under top-surface illumination at Brewster's angle of incidence. The photocurrent resonance is peaked at 2.8  $\mu\text{m}$  wavelength, i.e. slightly blue-shifted with respect to the ISB absorption peak. The photocurrent persists up to 320 K. The peak responsivity at 77 K was calibrated to be 0.15 mA/W under this illumination condition. This rather low value of our first prototype can be strongly enhanced by improving the design, the growth, the fabrication as well as the illumination conditions.

## 2. QCD DESIGN

The design of the ZnO/Zn<sub>0.6</sub>Mg<sub>0.4</sub>O QCD is shown in Figure 2. The simulation has been carried out by self-consistently solving the Schrödinger-Poisson equation using the effective mass approximation. The layer thickness sequence for one period starting from the active QW is 2.6/1.5/0.9/1.5/1.2/1.3/1.7/1.2 where bold figures correspond to the ZnMgO barriers. The 2.6 nm thick active QW is n-doped at a concentration of  $2 \times 10^{19} \text{ cm}^{-3}$  in order to populate the ground state with electrons.

As seen in Fig. 2, this design provides a significant envelope function overlap of the excited state of the active QW with the first extractor QW state in order to ensure a fast electron transfer within the extractor. The target wavelength of this design is 3.7  $\mu\text{m}$ .

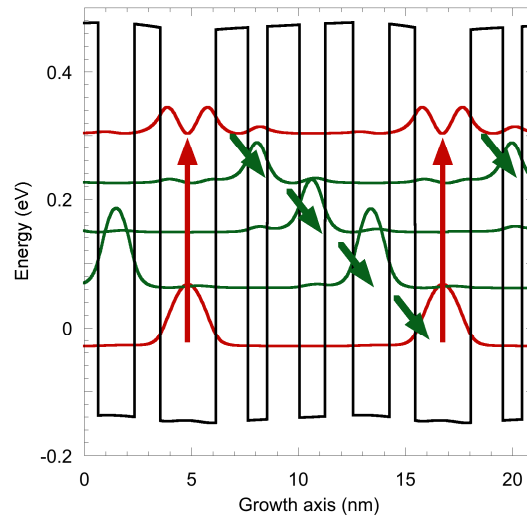


Figure 2. Conduction band profile of one period of the ZnO/Zn<sub>0.6</sub>Mg<sub>0.4</sub>O QCD. The red arrows show the intersubband absorption in the active QW while the green arrows show the electron scattering paths in the extractor.

### 3. SAMPLE GROWTH

The sample was grown on m-oriented ZnO substrates (Crystec) in a MBE system equipped with zinc (Zn) and magnesium (Mg) cells and one gallium (Ga) cell for n-type doping. Prior to growth, the substrates were annealed at 1065 °C under an oxygen (O) atmosphere to reveal the atomic steps. The atomic oxygen was provided by a plasma cell operating at 420 W with an oxygen-flow of 0.3 sccm. The substrate temperature was set to 420 °C during the growth. The Zn and O fluxes were adjusted to be close to stoichiometry to limit the defect concentration and resulted in a growth rate of 170 nm/h. The 2.6 nm thick active QWs were n-doped with Ga at a concentration of  $2 \times 10^{19} \text{ cm}^{-3}$ . The 20 period active region was grown on top of a 1  $\mu\text{m}$  thick ZnO bottom contact layer doped with Ga at  $2 \times 10^{19} \text{ cm}^{-3}$  and was capped with a 100 nm thick top ZnO contact layer Ga-doped at the same concentration. An optical inspection reveals no cracks in the sample after growth. The sample was investigated by X-ray diffraction spectroscopy (XRD). The period of the active region is found to be close to the nominal thickness within one monolayer (0.23 nm).

Similar samples consisting of ZnO/ZnMgO superlattices were investigated by scanning transmission electron microscopy (STEM) and atomic probe tomography (APT).<sup>16</sup> These structural characterizations confirm that the interfaces are abrupt and that the actual thickness of the ZnO QWs is within  $\pm 1$  monolayer close to the nominal thickness. However, due to the different adatom diffusion during growth along the c- and a-axis in the plane of the layers, a spatially coherent corrugation develops starting from the bottom contact layer up to the cap layer. In addition, APT reveals that the Mg concentration in the barriers varies by  $\pm 10\%$  in absolute values at the bottom and the top of the corrugations.

### 4. OPTICAL SPECTROSCOPY

The infrared transmission of the sample was probed using a Fourier transform infrared spectrometer. The sample was mechanically polished with facets at 45° angle to form a multi-pass waveguide with two internal reflections. Figure 3 shows the TM-polarized transmission divided by the TE transmission at 77 K and 300 K. The TM-polarized ISB absorption is peaked at 416 meV (2.98  $\mu\text{m}$  wavelength) with a full width at half maximum (FWHM) of 112 meV at 77 K. The peak absorption is blue-shifted with respect to the design target wavelength. This is a consequence of the depolarization shift. This effect is quite large because of the rather high doping of the active QW and large effective mass of ZnO.<sup>17</sup> Simulations accounting for this effect together with Poisson and exchange correlation,<sup>17</sup> and using the experimentally observed broadening of the transition, predict a peak absorption at 3  $\mu\text{m}$  wavelength, in agreement with the experimental value. The absorbance per QW is on the order of  $5.8 \times 10^{-3}$ .

Based on the calculated 0.6 nm ISB dipole length and on the experimental FWHM, the 2D electron density in the active QW is estimated to be  $4.6 \times 10^{12} \text{ cm}^{-2}$ . The latter value corresponds to a  $1.8 \times 10^{19} \text{ cm}^{-3}$  volume concentration which is close to the nominal doping concentration. The Fermi energy with respect to the ground state of the active QW is deduced to be 45.7 meV at 77 K.

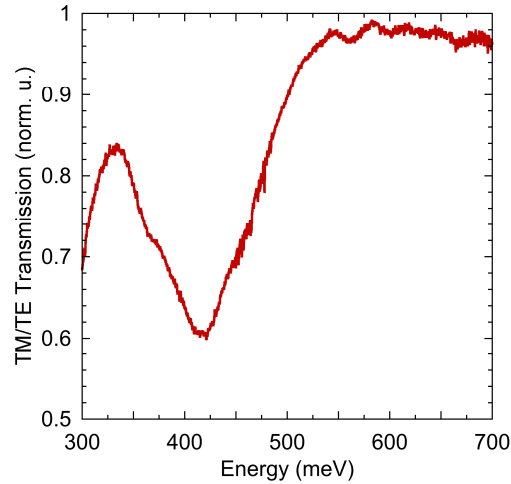


Figure 3. Transmission spectrum at 77 K of the QCD sample for TM polarized light divided by the spectrum for TE- polarized light.

### 5. DEVICE PROCESSING AND ELECTRICAL CHARACTERIZATIONS

The  $10 \times 10 \text{ mm}^2$  sample was processed as 260 square mesas with a size of  $10 \times 10$ ,  $20 \times 20$ ,  $30 \times 30$ ,  $50 \times 50$ ,  $75 \times 75$  and  $100 \times 100 \text{ }\mu\text{m}^2$ , respectively. The metallization of the top contact was restricted to the perimeter of the mesa in order to allow surface illumination at Brewster's angle of incidence ( $62^\circ$ ). In order to suppress the surface leakage currents, the devices were treated with  $\text{H}_2\text{O}_2$  at  $95^\circ\text{C}$  after etching of the mesas in a  $\text{CH}_4$ -based reactive ion etching plasma.<sup>18</sup> Figure 4 shows optical microscope images of the processed devices.

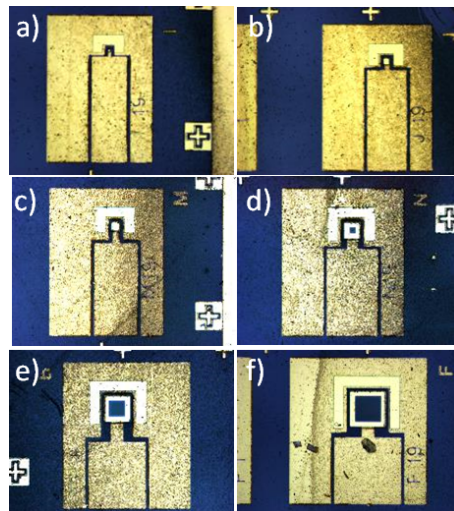


Figure 4. Top-view optical microscope images of various size QCDs after processing.

The I-V characteristics performed on all mesas reveal that 86% of all QCD devices are operational. Figure 5 left shows the I-V characteristics measured at room temperature of various QCDs with a size of  $100 \times 100 \mu\text{m}^2$ . One can notice a negligible dispersion between the I-V curves of the various QCDs. The resistance at zero bias,  $R_0$ , is in the range of 1.42-1.52 k $\Omega$  at 300 K. Figure 5 right presents the current density versus voltage (J-V) characteristics at 300 K for all sizes of QCDs. The absence of dispersion between the curves is a clear indication that the current is proportional to the surface and consequently that the sidewall leakage is negligible at room temperature thanks to the passivation procedure. When decreasing the temperature down to 77 K, the J-V characteristics of all mesa sizes are no more proportional to the surface. The I-V characteristics are found to be proportional to the mesa perimeter. This is a clear indication that the current at low temperatures is dominated by sidewall leakages. In addition,  $R_0$  is found to be inversely proportional to the mesa perimeter and not to the mesa surface. The  $R_0$  value increases from 71.7 k $\Omega$  (1.52 k $\Omega$ ) at 300 K to 1.75 M $\Omega$  (0.18 M $\Omega$ ) at 77 K for the  $10 \times 10 \mu\text{m}^2$  ( $100 \times 100 \mu\text{m}^2$ ) mesas, respectively. An Arrhenius plot of  $R_0 A$  reveals an activation energy at room temperature around 180 meV. This activation energy value at 300 K is close to the energy difference between the ground state of the first extractor and the ground state of the active QW.<sup>13</sup> This means that the resistance at zero bias at room temperature is limited by the non-resonant tunneling from the ground state of the active QW to the first extractor QW state.

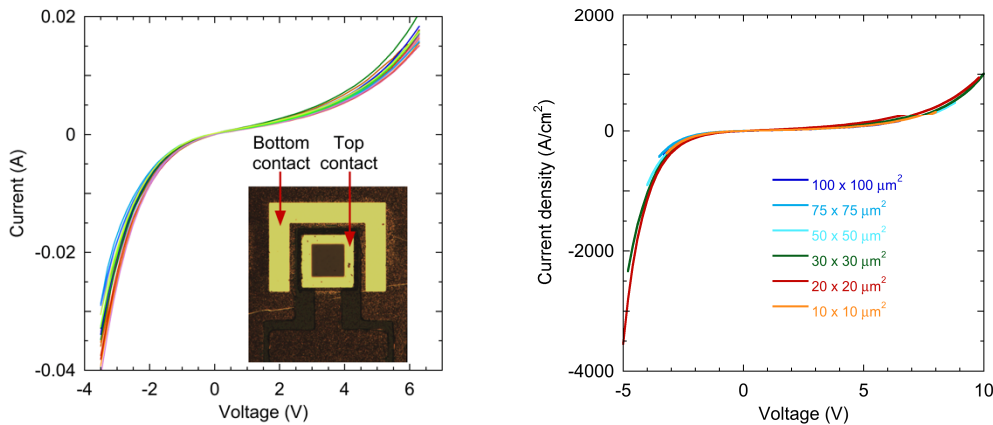


Figure 5. (left) I-V characteristics at 300 K of 17  $100 \times 100 \mu\text{m}^2$  QCD devices. The inset shows a top-view optical image of one of the QCD. (right) J-V characteristics of all size QCD functional devices at room temperature.

## 6. QCD DEVICE CHARACTERIZATION

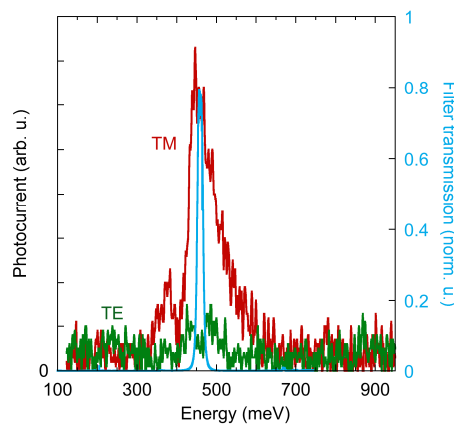


Figure 6. Photocurrent spectra at 77 K for TM- (red curve) and TE- (green curve) polarized light of a  $100 \times 100 \mu\text{m}^2$  QCD. The dip at 400 meV is due to  $\text{CO}_2$  absorption. The transmission spectrum of the filter is shown by the blue curve.

Photocurrent (PC) spectroscopy was performed on the  $100 \times 100 \mu\text{m}^2$  mesas QCDs using the FTIR spectrometer. The glow-bar source was mechanically chopped and a lock-in amplifier was used to detect the photoresponse of the QCDs. The QCDs were surface illuminated at Brewster's angle of incidence with a 10 cm focal length parabolic mirror. Figure 5 shows the photocurrent spectra for TM- and TE-polarized light at 77 K. The photocurrent spectrum is strongly TM-polarized as expected from a detector relying on ISB absorption. The residual TE-polarized signal may originate from diffraction effects on the facets of the mesas. The PC spectra are peaked at  $2.8 \mu\text{m}$  wavelength (443 meV) with a FWHM of 97 meV. The PC spectrum is blue-shifted with respect to the absorption spectra. The narrower linewidth and the spectral shift suggest that the electron transfer between the active QWs and the extractor region may be favored in the plane of the layers in barrier regions containing a higher Mg content. The photocurrent persists up to room temperature.

The responsivity of a typical device was calibrated under illumination by a  $1200^\circ \text{C}$  black-body source and using a narrow band-pass filter centered at  $2.7 \mu\text{m}$  wavelength close to the PC peak wavelength. The results corrected for the filter and cryostat window transmissions as well as the spot size onto the detector reveal a peak responsivity for TM-polarized light on the order of 0.15 mA/W under illumination of the top surface at Brewster's angle of incidence. Note that this value could be enhanced by both increasing the doping of the active QWs and making use of a grating or a  $45^\circ$  wedge configuration. The response could also be improved by more than two orders of magnitude using a waveguide configuration for a perfect TM coupling and complete absorption.<sup>15, 19</sup>

Based on the responsivity, one can estimate the transfer efficiency defined as the ratio of the photocurrent to the sum of the photocurrent and the parasitic current arising from electrons in the excited state relaxing back to the ground state of the same active QW.<sup>15</sup> The transfer efficiency is found to be of the order of  $\sim 1.15\%$ . Based on simulations, the Mg content fluctuation in the barriers appears as the main factor leading to the rather low transfer efficiency value of this prototype device. This value can be strongly enhanced by optimizing the design and growth of the QCD structure.

## 7. CONCLUSION

We have demonstrated the first QCDs based on m-plane ZnO/ZnMgO QWs grown by molecular beam epitaxy. The TM-polarized ISB absorption in the active QWs is peaked at  $3 \mu\text{m}$  wavelength, blue-shifted from the target wavelength of  $3.7 \mu\text{m}$  because of the depolarization shift. The QCD sample has been processed in the form of 260 square mesas with various mesa sizes. Special attention has been dedicated to the mesa facet passivation. I-V characteristics reveal that 86% of the devices are operational and that the surface leakage current is negligible at room temperature, which is not the case at 77 K. Photocurrent spectroscopy reveals a photocurrent resonance at  $2.8 \mu\text{m}$  wavelength, i.e. slightly blue-shifted with respect to the ISB absorption peak. The photocurrent persists up to room temperature. The calibrated peak responsivity at 77 K amounts to 0.15 mA/W under irradiation at Brewster's angle of incidence. The transfer efficiency of electrons between successive periods is estimated to be around 1.15 % and could be enhanced by optimizing the design and growth of the QCD structure.

## ACKNOWLEDGMENT

This work was funded by the European Union's Horizon 2020 Research and Innovation FET-Open Program under Grant Agreement No. 665107 (project ZOTERAC).

## REFERENCES

- [1] M. Belmoubarik, K Ohtani, and H Ohno, Appl. Phys. Lett. **92**, 191906 (2008).
- [2] N. Le Biavan, M. Hugues, M. Montes Bajo, J. Tamayo- Arriola, A. Jollivet, D. Lefebvre, Y. Cordier, B. Vinter, F.-H. Julien, A. Hierro, and J.-M. Chauveau, Appl. Phys. Lett. **111**, 231903 (2017).
- [3] L. Gendron, M. Carras, A. Huynh, V. Ortiz, C. Koeniguer, and V. Berger, Appl. Phys. Lett. **85**, 2824 (2004).
- [4] M. Graf, G. Scalari, D. Hoffstetter, J. Faist, H. Beere, E. Lindfield, D. Ritchie, and G. Davies, Appl. Phys. Lett. **84**, 475 (2004).
- [5] F. R. Giorgetta, E. Baumann, D. Hofstetter, C. Manz, Q. Yang, K. Kohler, and M. Graf, Appl. Phys. Lett. **91**, 111115 (2007).

- [6] F. R. Giorgetta, E. Baumann, M. Graf, Q. K. Yang, C. Manz, K. Kohler, H. E. Beere, D. A. Ritchie, E. Linfield, A. G. Davies, Y. Fedoryshyn, H. Jackel, M. Fischer, J. Faist, and D. Hofstetter, *IEEE J. Quantum Electron.* **45**, 1029–1042 (2009), and reference therein.
- [6] A. Buffaz, M. Carras, L. Doyennette, A. Nedelcu, X. Marcadet, and V. Berger, *Appl. Phys. Lett.* **96**, 172101 (2010).
- [7] A. Vardi, G. Bahir, F. Guillot, C. Bougerol, E. Monroy, S. E. Schacham, M. Tchernycheva, and F. H. Julien, *Appl. Phys. Lett.* **92**, 011112 (2008).
- [8] A. Vardi, N. Kheirodin, L. Nevou, H. Machhadani, L. Vivien, P. Crozat, M. Tchernycheva, R. Colombelli, F. H. Julien, F. Guillot, C. Bougerol, E. Monroy, S. Schacham, and G. Bahir, *Appl. Phys. Lett.* **93**, 193509 (2008).
- [9] S. Sakr, Y. Katsov, S. Haddadi, M. Tchernycheva, L. Vivien, I. Sarigianni-dou, N. Isac, E. Monroy, and F. H. Julien, *Electron. Lett.* **46**, 1685 (2010).
- [10] S. Sakr, E. Giraud, A. Dussaigne, M. Tchernycheva, N. Grandjean, and F. H. Julien, *Appl. Phys. Lett.* **100**, 181103 (2012).
- [11] S. Sakr, E. Giraud, M. Tchernycheva, N. Isac, P. Quach, E. Warde, N. Grandjean, and F. H. Julien, *Appl. Phys. Lett.* **101**, 251101 (2012).
- [12] A. P. Ravikumar, J. De Jesus, M. C. Tamargo, C. F. Gmachl, *Appl. Phys. Lett.* **107**, 141105 (2015).
- [13] A. Gomez, N. Péré-Laperne, L.-A. de Vaulchier, C. Koeniguer, A. Vasanelli, A. Nedelcu, X. Marcadet, Y. Guldner, and Vincent Berger, *Phys. Rev. B* **77**, 085307 (2008).
- [14] A. Vardi, S. Sakr, J. Mangeney, K. W. Kandaswamy, E. Monroy, M. Tchernycheva, S. E. Schacham, F. H. Julien, and G. Bahir, *Appl. Phys. Lett.* **99**, 202111 (2011).
- [15] S. Sakr, P. Crozat, D. Gacemi, Y. Kotsar, A. Pesach, P. Quach, N. Isac, M. Tchernycheva, L. Vivien, G. Bahir, E. Monroy, F. H. Julien, *Appl. Phys. Lett.* **102**, 011135 (2013).
- [16] E. Di Russo, L. Mancini, F. Moyon, S. Moldovan, J. Houard, F.H. Julien, M. Tchernycheva, J.-M. Chauveau, M. Hugues, G. Da Costa, I. Blum, W. Lefebvre, D. Blavette, L. Rigutti, *Appl. Phys. Lett.* **111**, 032108 (2017).
- [17] M. Montes Bajo, J. Tamayo-Arriola, M. Hugues, J. M. Ulloa, N. Le Biavan, R. Peretti, F. H. Julien, J. Faist, J.-M. Chauveau, and A. Hierro, *Phys. Rev. Appl.* **10**, 024005 (2018).
- [18] S.-W. Na, M. H. Shin, Y. M. Chung, J. G. Han, and N.-E. Lee, *Journ. of Vacuum Science & Technology A*, **23**, 898 (2005).
- [19] B. Schwarz, P. Reininger, A. Harrer, D. MacFarland, He. Detz, A. M. Andrews, W. Schrenk, and G. Strasser, *Appl. Phys. Lett.* **111**, 061107 (2017).